Phytochemistry 242 (2026) 114692

Contents lists available at ScienceDirect

Phytochemistry

journal homepage: www.elsevier.com/locate/phytochem

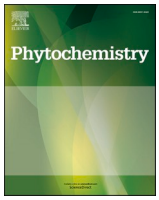

Functional characterization and directed evolution of *Cicer arietinum* glutathione transferases for enhanced hydroperoxidase activity and ligandin function

Anni Kontouri [a], Nikolaos Georgakis [a], Anastassios C. Papageorgiou [b], Nikolaos E. Labrou [a,*]

[a] Laboratory of Enzyme Technology, Department of Biotechnology, School of Applied Biology and Biotechnology, Agricultural University of Athens, 75 Iera Odos Street, GR-11855, Athens, Greece
[b] Turku Bioscience Centre, University of Turku and Åbo Akademi University, Turku, 20521, Finland

ARTICLE INFO

Keywords:
Cicer arietinum
Fabaceae
Directed evolution
DNA shuffling
Hydroperoxidase activity
Pesticide binding
Glutathione transferases
Xenobiotic detoxification

ABSTRACT

Tau class glutathione transferases (GSTUs) play essential roles in plant defense by facilitating the nucleophilic attack of glutathione (GSH) to a wide range of electrophilic xenobiotics. In addition to their conjugating activity, these enzymes possess hydroperoxidase function, enabling the detoxification of harmful organic hydroperoxides into less reactive alcohols. In this study, we identified three closely related GST isoenzymes (96–98 % sequence identity) from *Cicer arietinum* (*Ca*GSTUs) through computational homology screening. Full-length cDNAs encoding these GSTs were cloned, recombinantly produced in *E. coli*, and purified for functional characterization. Enzyme kinetics were evaluated using model substrates, cumene hydroperoxide (CuOOH) and 1-chloro-2,4-dinitrobenzene (CDNB), revealing that *Ca*GSTU1-1 displayed superior hydroperoxidase activity and thermal stability. Based on these properties, *Ca*GSTU1-1 was selected as the parental scaffold for directed evolution via DNA shuffling, using the homologous *Glycine* max isoenzyme *Gm*GSTU4-4. Screening of the generated chimeric library resulted in the identification of a new variant, *CaGm*GSTU, which demonstrated a fourfold enhancement in catalytic turnover and efficiency toward both substrates. Additionally, *CaGm*GSTU exhibited altered ligand-binding characteristics, including increased affinity for selected pesticides. Structural modeling and viscosity-dependence kinetics indicated that these enhancements were primarily driven by changes in enzyme flexibility. Given the widespread toxicity of hydroperoxides and related pollutants, *CaGm*GSTU represents a promising tool for detoxification applications in environmental and agricultural biotechnology.

1. Introduction

GSTs comprise a heterogeneous family of enzymes involved in multiple physiological and detoxification processes. In plant systems, GSTs are widely recognized for their ability to catalyze the conjugation of GSH to a broad spectrum of endogenous and exogenous electrophilic compounds, thereby facilitating detoxification (Labrou et al., 2015; Cassier-Chauvat et al., 2023). Beyond this conjugation activity, many plant GSTs also function as hydroperoxidases, enabling the reduction of organic hydroperoxides to less harmful alcohols (Gallé et al., 2021). Their expression is highly responsive to environmental stresses, including both abiotic and biotic, underscoring their involvement in plant stress adaptation. Additionally, GSTs contribute to diverse physiological processes such as primary and secondary metabolism, signal transduction, and homeostasis, even under non-stress conditions (Labrou et al., 2015; Horváth et al., 2023). In addition, they have been associated with significant adaptive traits, including herbicide resistance in plants, pesticide resistance in insects, and drug resistance mechanisms in humans (Micic et al., 2024; Zhang et al., 2025; Xu et al., 2025).

Plant GSTs are classified into several distinct classes based on phylogenetic relationships, gene structure, and overall protein architecture. These classes include dehydroascorbate reductase (DHAR), elongation factor 1Bγ (EF1Bγ), glutathionyl hydroquinone reductase (GHR), Phi (GSTF), Hemerythrin (GSTH), Iota (GSTI), Lambda (GSTL), Theta (GSTT), Tau (GSTU), Zeta (GSTZ), microsomal prostaglandin E synthase type 2 (mPGES-2), tetrachloro-hydroquinone dehalogenase (TCHQD), and Ure2p-like proteins (Lallement et al., 2014;

* Corresponding author.
E-mail address: Lambrou@aua.gr (N.E. Labrou).

https://doi.org/10.1016/j.phytochem.2025.114692
Received 12 June 2025; Received in revised form 26 September 2025; Accepted 26 September 2025
Available online 27 September 2025

Sylvestre-Gonon et al., 2019). While most GSTs function as dimers, GSTLs, GHRs, and DHARs are exceptions, typically existing as monomeric enzymes. Each monomer is organized into two domains with distinct roles and structural features. The N-terminal domain resembles the thioredoxin fold, characterized by a βαβαβα motif, and houses the GSH-binding site (G-site). The C-terminal domain, predominantly α-helical, contributes to substrate recognition through the formation of the hydrophobic substrate-binding site (H-site) (Sylvestre-Gonon et al., 2019). Catalytic residues, typically tyrosine, serine, or cysteine, within the N-terminal domain, activate the thiol group of GSH to be at least partially under the thiolate form at physiological pH range of 6–7 (Lallement et al., 2014; Mannervik, 2023). GSTs belonging to the same class typically share more than 40 % amino acid sequence identity, whereas those from different classes generally exhibit less than 25 % sequence identity (Oakley, 2011). Despite this divergence, the overall three-dimensional structure of GSTs remains highly conserved across classes. This structural conservation, coupled with significant active-site plasticity, underlies the broad substrate specificity and functional versatility of GST enzymes (Labrou et al., 2015; Kontouri et al., 2024).

In plants, the majority of GSTs belong to the Phi (GSTF) and Tau (GSTU) classes, which represent the most thoroughly characterized classes to date. Both GSTFs and GSTUs are known for their broad substrate specificity and are critically involved in the detoxification of xenobiotic compounds, including a wide range of herbicides and pesticides (Neuefeind et al., 1997; Dixon et al., 2002). Their ability to conjugate GSH to diverse electrophilic substrates plays a central role in safeguarding plant cells from chemical stress. Importantly, these enzymes have been associated with multiple herbicide resistance (MHR) in agricultural weeds, a phenomenon attributed to enhanced metabolic detoxification driven by the upregulation or functional adaptation of endogenous GSTs (Dixon et al., 2002).

GSTs are widely recognized as valuable platforms for protein engineering, owing to their broad substrate scope, modular domain organization, comprising discrete GSH-binding (G-site) and hydrophobic substrate-binding (H-site) regions, and the ease with which they can be expressed and purified in *E. coli* systems (Perperopoulou et al., 2018). Engineered GSTs, particularly those involved in pesticide detoxification, provide critical insight into the molecular underpinnings of xenobiotic metabolism and resistance evolution in plants and other organisms (Chronopoulou et al., 2018). Numerous studies have utilized approaches such as site-directed mutagenesis and directed evolution to dissect the structural and functional determinants of GST activity. For instance, Dixon et al. (2003) employed DNA shuffling and subsequent mutagenesis of *Zea mays* Tau class GST genes to generate variants with a 29-fold enhancement in fluorodifen detoxification. Similarly, Axarli et al. (2016) applied DNA shuffling to homologous Tau GSTs from *Glycine max*, yielding chimeric enzymes with atypical allosteric behaviour and significantly improved catalytic efficiency against the same herbicide. In another study, Axarli et al. (2017) constructed a recombinant library of alpha-class GSTs by combining human (hGSTA1-1) and rat (rGSTA1-1) genes. Screening of this library identified a chimeric form (GSTD4) with superior GSH-binding affinity, enhanced turnover, and elevated thermal stability. Structural analysis of GSTD4 revealed subtle conformational shifts in the G-site, and further optimization through site-saturation mutagenesis at position Cys112 (Cys112Ser) led to increased oxidative resistance and catalytic performance. Additionally, Chronopoulou et al. (2018) developed a GSTU variant from *Phaseolus vulgaris* and *Glycine max*, using cDNA derived from stress-treated tissues, resulting in an enzyme with enhanced glutathione peroxidase activity and atypical kinetics toward CDNB. More recently, directed evolution efforts by Ioannou et al. (2022) and Axarli et al. (2023) have yielded highly efficient engineered Phi and Tau GST variants with markedly improved detoxification capacities.

Cicer arietinum (chickpea) is a globally significant legume, valued for its high protein content and dense nutritional composition, which contribute to both human health and agricultural sustainability (Silva et al., 2025). Recent studies have highlighted its potential in promoting eco-friendly agricultural practices and supporting food security, particularly in regions facing climatic and resource challenges (Akchaya et al., 2025). To strengthen stress resilience and optimize productivity, a deeper understanding of the species' detoxification systems is critical (Asati et al., 2024). In this context, the present study investigates the functional roles of three previously uncharacterized GST isoenzymes from *C. arietinum*, with a focus on their contributions to stress response and xenobiotic metabolism. Additionally, through directed evolution, a novel chimeric variant, (*Ca*Gm*GSTU*), exhibiting markedly enhanced hydroperoxidase activity and modified ligand-binding behaviour was found and characterised. Given the toxicity and prevalence of organic hydroperoxides in both agricultural and environmental settings, *Ca*Gm*GSTU* holds promise as an effective biocatalyst for detoxification, with potential applications in plant biotechnology and environmental bioremediation.

2. Results and discussion

2.1. Identification, cloning, expression of CaGSTUs

Previous studies have established that the Tau class GST isoenzyme *Gm*GSTU4-4 from *Glycine* max exhibits significant hydroperoxidase activity and plays a key role in cellular detoxification and antioxidant defense mechanisms (Axarli et al., 2009a, 2016, 2023). To explore the catalytic diversity of homologous GSTUs in *C. arietinum*, a BLASTp analysis was performed using the *Gm*GSTU4-4 amino acid sequence (UniProt ID: O49235) as the query. Several candidate GST sequences were identified in the *C. arietinum* genome and further evaluated through BLASTn searches in the Chickpea Transcriptome Database (CTDB; Verma et al., 2015).

Among the identified candidates, three uncharacterized GST isoenzymes, designated *Ca*GSTU1-1, *Ca*GSTU2-2, and *Ca*GSTU3-3, exhibiting amino acid sequence identities ranging from 64.3 % to 33.8 %, were selected for experimental characterization (Fig. 1A). Transcriptomic data revealed that the corresponding mRNAs are upregulated under salinity stress conditions. This is consistent with findings by Kaur et al. (2022), who reported elevated levels of hydrogen peroxide and malondialdehyde in salt-stressed *C. arietinum*, indicative of oxidative stress. Notably, *Ca*GSTU1-1 and *Ca*GSTU2-2 transcripts were also found to be overexpressed in chickpea tissues subjected to drought stress and *Fusarium* wilt infection, suggesting a potential multifunctional role for these enzymes in mediating responses to both abiotic and biotic stressors.

To assess the evolutionary relationships of the three *Ca*GSTs, a phylogenetic analysis was conducted alongside representative members of known GST classes from various plant sources. The resulting tree, shown in Fig. 1B, clearly places all three *Ca*GSTUs within the Tau class (GSTU), a major plant-specific GST subclass associated with detoxification and stress responses. *Ca*GSTU1-1 clusters closely with a Tau class GST from *Medicago truncatula* (*Mt*GSTU47, Accession No: AUW37507.1) sharing a SeqID 86.3 %. *Mt*GSTU47 shows gene expression in all plant tissues under normal growth or stress conditions and exhibits wide substrate specificity. Experimental evidence supports the protective role of *Mt*GSTUs in plant cell physiology (Han et al., 2018). Additionally, *At*GSTU19 (Accession No: NP_565178.1) clusters in a neighboring clade of Tau class GSTs, supporting the functional similarity of *Ca*GSTU1-1 with other Tau class members from *Arabidopsis*. Gene expression analysis using microarray datasets indicated that *At*GSTU19 is broadly expressed across most *Arabidopsis* tissues and exhibits the highest transcript abundance among Tau class GSTs (Zimmermann et al., 2004). Studies involving transgenic Arabidopsis plants with elevated AtGSTU19 expression have demonstrated significantly improved tolerance to salt and drought stress, along with protection against methyl viologen-induced oxidative damage. These findings suggest that *At*GSTU19 plays a regulatory role in abiotic stress responses, potentially by

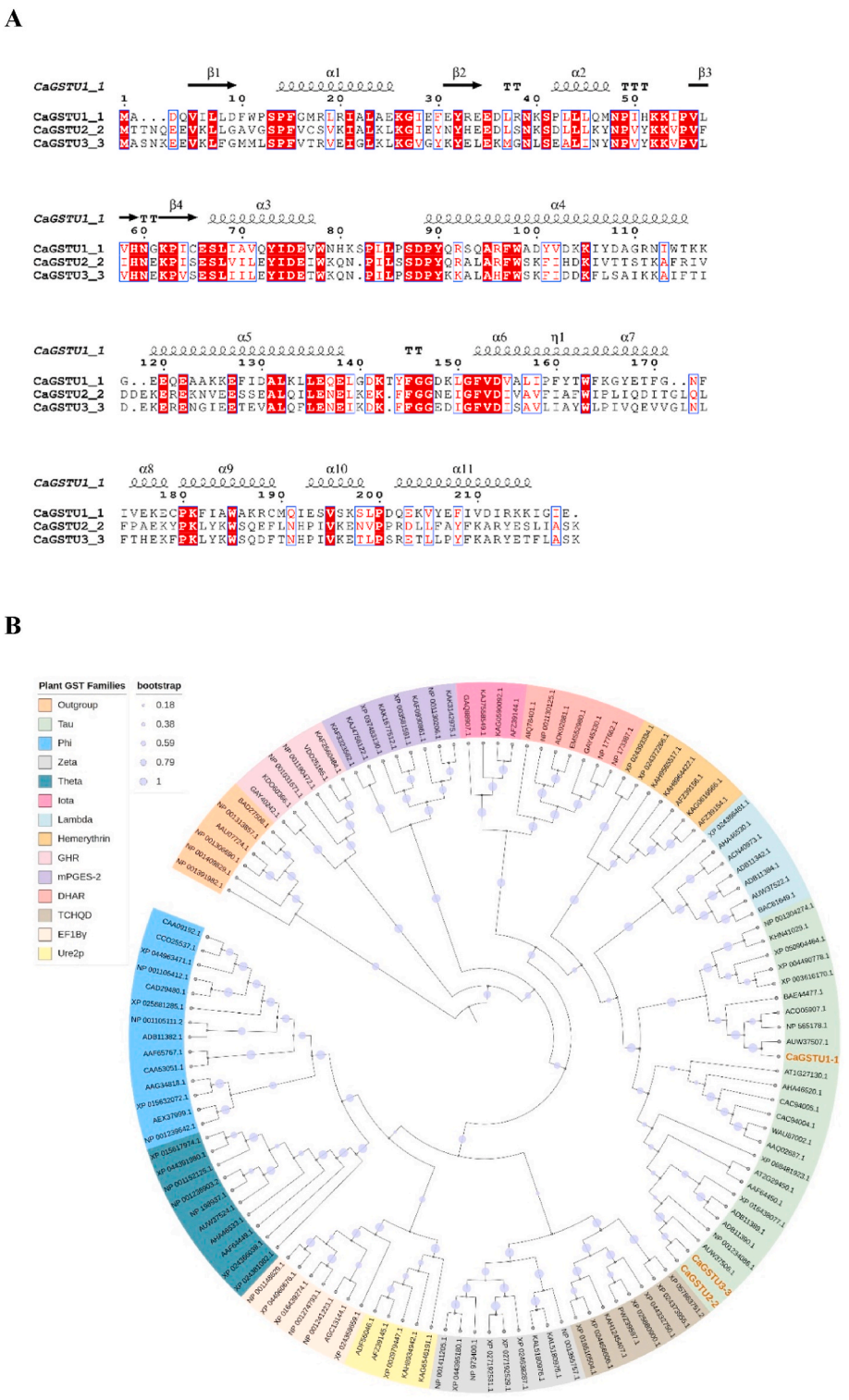

Fig. 1. Sequence alignment and phylogenetic analysis of *Ca*GSTUs. (A) Multiple sequence alignment of *Ca*GSTU1-1, *Ca*GSTU2-2, and *Ca*GSTU3-3 was performed using CLUSTAL Omega (Sievers and Higgins, 2018) and visualized with ESPript 3.0 (Robert and Gouet, 2014). The alignment is annotated with the predicted secondary structure of *Ca*GSTU1-1, where α-helices are depicted as coils, β-strands as arrows, and β-turns are indicated as "TT." Residue numbering corresponds to *Ca*GSTU1-1. Conserved residues are shaded, and columns with ≥70 % similarity based on physicochemical properties are boxed. GenBank accession numbers: *Ca*GSTU1-1 (ALZ41811.1), *Ca*GSTU2-2 (ALZ41812.1), *Ca*GSTU3-3 (ALZ41813.1). **(B)** Phylogenetic tree showing the relationship of *Ca*GSTUs (highlighted in red) with members of known plant GST classes including Phi (GSTF), Tau (GSTU), Lambda (GSTL), Theta (GSTT), Zeta (GSTZ), Iota (GSTI), Dehydroascorbate Reductase (DHAR), Tetrachloro-hydroquinone Dehalogenase (TCHQD), Microsomal prostaglandin E synthase type 2 (mPGES-2), Elongation factor 1Bγ (EF1Bγ), Glutathionyl hydroquinone reductase (GHR), Hemerythrin (GSTH), Ure2p, and an outgroup of protein sequences to support better clustering results. The amino acid sequences used in the analysis are provided in the Supplementary file. Sequence alignment was carried out using CLUSTAL Omega. The phylogenetic tree was constructed with the UPGMA method with the JTT model, and the branches were evaluated for their robustness using the bootstrap test with 500 replications. Evolutionary analyses were conducted in MEGA12 (Kumar et al., 2024) and visualized using iTOL v5 (Letunic and Bork, 2021). (For interpretation of the references to color in this figure legend, the reader is referred to the Web version of this article.)

stimulating antioxidant enzyme activity and thereby contributing to reactive oxygen species (ROS) detoxification and redox homeostasis (Roxas et al., 2000). *Ca*GSTU2-2 and *Ca*GSTU3-3, while also grouping within the Tau clade, are located in a distinct sub-branch, suggesting greater sequence divergence and possibly specialized functional roles. Their clustering with another GSTU from *Medicago truncatula* (*Mt*GSTU46, Accession No: AUW37506.1) and different GSTUs (e.g. GSTU43 from *Solanum lycopersicum*, Accession No: NP_001234086.1 or GSTUs from *Populus trichocarpa*, Accession No: ADB11389.1 and ADB11390.1) implies that they may differ in substrate specificity, regulation, or physiological function. For example, *Mt*GSTU46 exhibits narrow substrate specificity in comparison with *Mt*GSTU47 which displays a broader spectrum of substrate specificity (Han et al., 2018). *Mt*GSTU46 expression levels are escalated when drought and salinity stress conditions occur (Hasan et al., 2021). What is more, Liu et al. (2019) found that GSTU43 plays an important role against low temperature-induced oxidative stress in tomato plants and, therefore, facilitates the redox homeostasis of plants.

Full-length cDNAs encoding the open reading frames (ORFs) of *Ca*GSTU1-1, *Ca*GSTU2-2, and *Ca*GSTU3-3 were amplified by RT-PCR from *C. arietinum* mRNA and subsequently cloned into the pEXP5-CT/TOPO®TA expression vector, which is driven by the T7 promoter. The constructs were transformed into *E. coli* for heterologous expression. *Ca*GSTU1-1 and *Ca*GSTU2-2 were successfully purified via single-step affinity chromatography using GSH-Sepharose resin. In contrast, *Ca*GSTU3-3 exhibited negligible binding to the GSH matrix and was instead purified by ion-exchange chromatography using DEAE-Sepharose with stepwise salt elution. The purity of all three recombinant enzymes is shown in Fig. S1.

2.2. Substrate specificity and kinetics analysis of CaGSTUs

The substrate specificity profiles of the *Ca*GSTU isoenzymes were evaluated using a panel of structurally diverse electrophilic substrates. As shown in Fig. 2, *Ca*GSTU1-1 exhibited the broadest substrate specificity and the highest activity across all tested substrates, particularly toward cumene hydroperoxide, *trans*-2-nonenal, and CDNB analogs. *Ca*GSTU2-2 showed moderate activity toward the halogenated substrates (CDNB and BDNB) and *trans*-2-nonenal but demonstrated relatively low activity toward hydroperoxides. *Ca*GSTU3-3 displayed the highest activity towards CDNB and BDNB but minimal activity toward hydroperoxides or *trans*-2-nonenal, indicating a narrower substrate range.

To further characterize their enzymatic properties, steady-state kinetic analysis was performed using GSH and CDNB as the electrophilic substrate (Fig. 3). Key parameters, including turnover number (k_{cat}) and Michaelis constant (K_m), were determined and are summarized in Table 1. Among the three isoenzymes, *Ca*GSTU1-1 exhibited the highest catalytic turnover ($k_{cat} = 694\ min^{-1}$), along with a moderate K_m for GSH (0.61 mM) and low K_m for CDNB (0.34 mM), resulting in high catalytic efficiencies (k_{cat}/K_m) of 1137.7 $mM^{-1}\ min^{-1}$ for GSH and 2041.2 $mM^{-1}\ min^{-1}$ for CDNB. *Ca*GSTU2-2 demonstrated intermediate activity ($k_{cat} = 346\ min^{-1}$) but a remarkably low K_m for GSH (0.17 mM), resulting in high k_{cat}/K_m value for GSH (2035.3 $mM^{-1}\ min^{-1}$). However, *Ca*GSTU2-2 displayed sigmoidal kinetics for CDNB, as indicated by an $S_{0.5}$ of 0.35 mM and a Hill coefficient of $n_H = 1.5 \pm 0.1$, suggesting positive cooperativity in substrate binding at the H-site. This behaviour reflects potential allosteric regulation or intersubunit communication. Such cooperative kinetics are characteristic of several tau and phi class GSTs and have been linked to intersubunit communication mediated through the dimer interface, as previously observed in crystallographic studies (Axarli et al., 2016; Ioannou et al., 2022). *Ca*GSTU3-3 displayed the lowest turnover rate (k_{cat} 206 min^{-1}), the highest K_m for GSH (0.82 mM), and the lowest catalytic efficiencies toward both substrates. The kinetic response to CDNB also showed sigmoidal behaviour ($S_{0.5} = 0.46$ mM; $n_H = 2.1 \pm 0.2$), indicating stronger cooperativity than *Ca*GSTU2-2. Despite this, the overall lower activity and catalytic efficiency (251.2 $mM^{-1}\ min^{-1}$ for GSH and 447.8 $mM^{-1}\ min^{-1}$ for CDNB) suggest that *Ca*GSTU3-3 may serve more specialized or regulatory roles rather than detoxification.

Collectively, these results highlight *Ca*GSTU1-1 as the most catalytically competent isoenzyme. The presence of cooperative kinetics in *Ca*GSTU2-2 and *Ca*GSTU3-3 further underscores the structural and functional diversity of tau-class GSTs in *C. arietinum* and points to potential regulatory roles in stress response through allosteric substrate modulation.

2.3. Thermal stability

The thermal stability of *Ca*GSTU1-1, *Ca*GSTU2-2, and *Ca*GSTU3-3 was evaluated through thermal denaturation assays (Fig. 4), which provide a rapid and effective means of determining enzyme stability under heat stress. The melting temperature (T_m), defined as the temperature at which 50 % of enzymatic activity is lost, was used as a metric for thermostability. As summarized in Table 2, all three isoenzymes exhibited substantial thermal resistance, with T_m values ranging from 63.5 °C to 69.9 °C. Among the three enzymes, *Ca*GSTU1-1 displayed the highest thermostability, with a T_m of 69.9 ± 0.7 °C, indicating

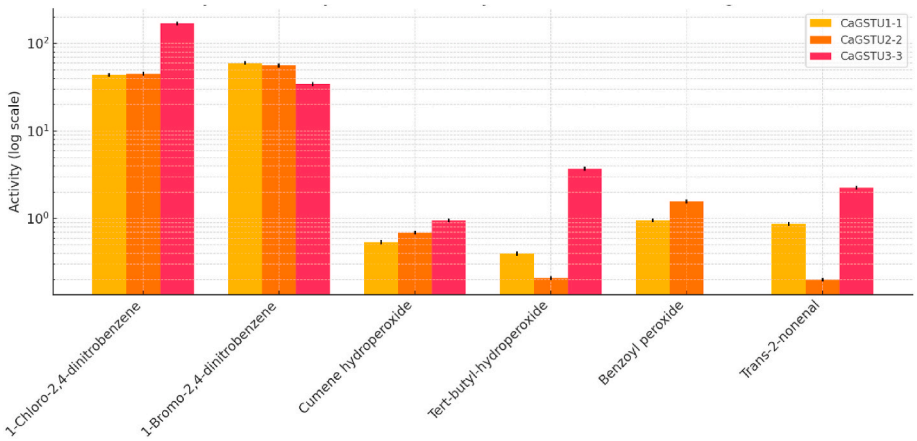

Fig. 2. Substrate specificity of *Ca*GSTUs. Enzymatic activity (units/mg) profiles of three *Ca*GST isoenzymes toward halogenated aromatic compounds (1-chloro-2,4-dinitrobenzene, 1-bromo-2,4-dinitrobenzene), hydroperoxides (cumene hydroperoxide, *tert*-butyl hydroperoxide, benzoyl hydroperoxide) and the alkenal *trans*-2-nonenal. Data are presented as mean values with error bars representing ± standard deviation. The y-axis is shown on a logarithmic scale to enhance visualization of differences across a wide range of activity levels. Assays were performed under standard conditions as described in the Materials and Methods section.

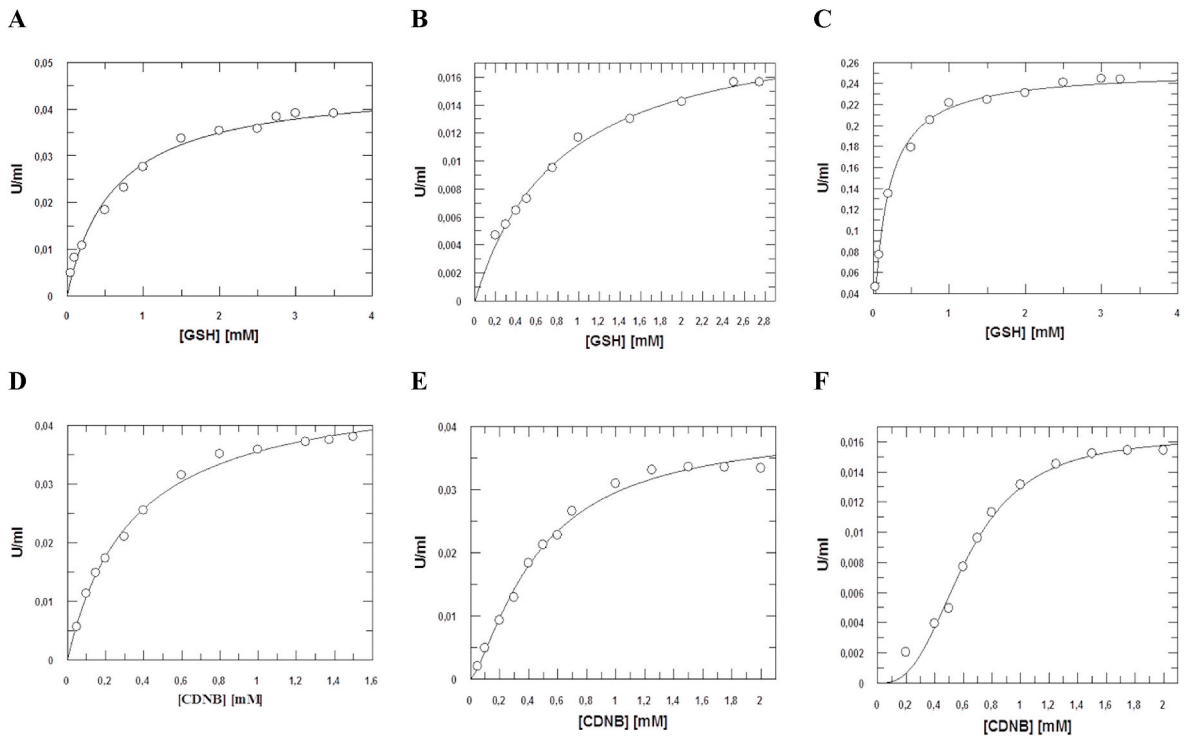

Fig. 3. Steady-state kinetic analysis of *Ca*GSTU isoenzymes using GSH and CDNB as substrates. Michaelis–Menten kinetics were evaluated for *Ca*GSTU1-1 (A, D), *Ca*GSTU2-2 (B, E), and *Ca*GSTU3-3 (C, F). **(A–C)** Reactions were performed using GSH as the variable substrate and 1-chloro-2,4-dinitrobenzene (CDNB) at a fixed, saturating concentration. **(D–F)** Reactions were performed using CDNB as the variable substrate while keeping GSH concentration fixed. Each data point represents the mean of three independent experiments conducted in triplicate. Kinetic parameters (K_m and k_{cat}) were derived by nonlinear regression fitting to the Michaelis–Menten equation, except in cases of observed sigmoidal kinetics, where the Hill equation was applied.

Table 1
Steady-state kinetic analysis of *Ca*GSTU1-1, *Ca*GSTU2-2 and *Ca*GSTU3-3 for the CDNB/GSH and substrate system.

Enzyme	k_{cat} (min^{-1})	K_m (mM) (GSH)	K_m (mM) (CDNB)	k_{cat}/K_m (mM^{-1} min^{-1}) (GSH)	k_{cat}/K_m (mM^{-1} min^{-1}) (CDNB)
***Ca*GSTU1-1**	694 ± 9.9	0.61 ± 0.07	0.34 ± 0.02	1137.73	2041.2
	k_{cat} (min^{-1})	**K_m (mM) (GSH)**	**$S_{0.5}$ (mM)[a] (CDNB)**	**k_{cat}/K_m (mM^{-1} min^{-1}) (GSH)**	**$k_{cat}/S_{0.5}$ (mM^{-1} min^{-1}) (CDNB)**
***Ca*GSTU2-2**	346 ± 16.2	0.17 ± 0.01	0.35 ± 0.06	2035.3	988.6
***Ca*GSTU3-3**	206 ± 4.0	0.82 ± 0.06	0.46 ± 0.17	251.2	447.8

[a] The Hill coefficients were $n_{H=}$1.5 ± 0.1 and 2.1 ± 0.2 for *Ca*GSTU2-2 and *Ca*GSTU3-3, respectively.

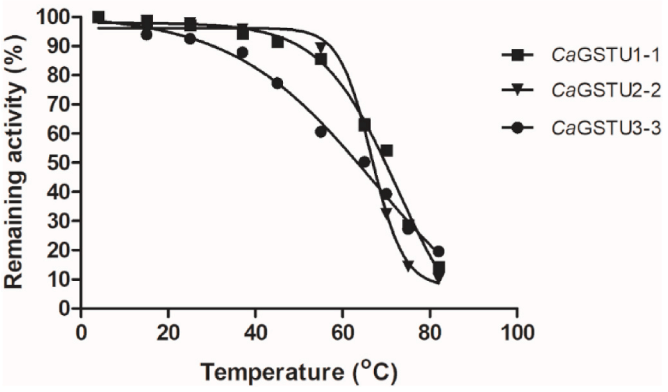

Fig. 4. Thermal inactivation profiles of *Ca*GSTU1-1, *Ca*GSTU2-2, and *Ca*GSTU3-3. The plot illustrates the thermal stability of *Ca*GSTU isoenzymes based on residual enzymatic activity following a 10 min incubation at varying temperatures (4–80 °C). Enzyme activity is expressed as a percentage of the initial activity measured at 25 °C. Data points represent the mean from three independent experiments. The melting temperature (T_m), defined as the temperature at which 50 % of enzyme activity is lost, was derived from the inactivation curve.

exceptional structural resilience under thermal stress. This value places *Ca*GSTU1-1 among the most thermostable plant GSTs reported to date (Axarli et al., 2017; Skopelitou et al., 2015), further supporting its selection as a robust candidate for protein engineering and biotechnological applications requiring enzyme function under elevated temperatures. *Ca*GSTU2-2 exhibited high thermal stability, with a T_m of 67.5 ± 0.8 °C, only slightly lower than *Ca*GSTU1-1. This suggests that it retains a relatively stable conformation under physiological and moderately elevated temperatures, potentially reflecting its functional role in stress environments. In contrast, *Ca*GSTU3-3 showed the lowest thermostability, with a T_m of 63.5 ± 1.4 °C, suggesting a more labile structure under thermal stress. The reduced thermal stability may be associated with lower catalytic activity and substrate affinity observed in kinetic analyses, further indicating that *Ca*GSTU3-3 may be specialized for functions not requiring prolonged activity under stress conditions.

2.4. Directed evolution

The most catalytically efficient and thermostable isoenzyme, *Ca*GSTU1-1, was selected for directed evolution alongside the Tau class *Gm*GSTU4-4 from *Glycine max*, which is well characterized for its high

Table 2
Melting temperatures of *Ca*GSTU1-1, *Ca*GSTU2-2 and *Ca*GSTU3-3 based on results from thermal denaturation studies.

Enzyme	T_m (°C)
***Ca*GSTU1-1**	69.9 ± 0.7
***Ca*GSTU2-2**	67.5 ± 0.8
***Ca*GSTU3-3**	63.5 ± 1.4

hydroperoxidase activity (Axarli et al., 2016, 2023). Using DNA shuffling (Arnold, 1998; Reetz et al., 2006; Axarli et al., 2016), a library of chimeric variants was constructed and screened for enhanced enzymatic activity (Fig. S2). Among the screened clones, one variant, designated *CaGm*GSTU, exhibited the highest specific activity and was selected for further characterization.

Sequence analysis of *CaGm*GSTU (Fig. 5) confirmed that it was primarily derived from *Ca*GSTU1-1, with incorporated sequence segments from *Gm*GSTU4-4. Notably, no spontaneous point mutations were detected. The recombinant *CaGm*GSTU protein was expressed in *E. coli*, purified to homogeneity (Fig. S3), and subjected to detailed kinetic characterization using CDNB and cumene hydroperoxide (CuOOH) as representative substrates (Table 3).

To evaluate the catalytic improvements achieved through directed evolution, steady-state kinetic parameters of the chimeric enzyme *CaGm*GSTU were compared with its parental isoform CaGSTU1-1 using two model substrates: the halogenated aromatic compound CDNB and the organic hydroperoxide CuOOH (Table 3). *CaGm*GSTU demonstrated a substantial increase in catalytic turnover, with a k_{cat} of 1300 min^{-1}, nearly double that of *Ca*GSTU1-1 (694 min^{-1}, Table 1). The enzyme maintained a similar K_m for GSH (0.60 mM) and a modest increase in K_m for CDNB (0.41 mM), suggesting that substrate binding affinity remained largely unchanged. Notably, the catalytic efficiency of *CaGm*GSTU was significantly enhanced, with k_{cat}/K_m values of 2166.7 mM^{-1} min^{-1} (GSH) and 3170.7 mM^{-1} min^{-1} (CDNB), outperforming the wild-type CaGSTU1-1 and establishing *CaGm*GSTU as a superior detoxifying enzyme in the CDNB assay system. When assayed with cumene hydroperoxide, a model hydroperoxide, *CaGm*GSTU exhibited a k_{cat} of 1470 min^{-1}, representing a ~4-fold enhancement relative to CaGSTU1-1 (k_{cat} = 370 min^{-1}). The K_m values for GSH were nearly identical (0.59 vs. 0.30 mM), while *CaGm*GSTU showed a slightly higher K_m for CuOOH (3.40 mM vs. 2.51 mM), indicating a modest decrease in substrate affinity. However, the overall catalytic efficiency toward CuOOH (k_{cat}/K_m = 432.4 mM^{-1} min^{-1}) was 2.9-fold greater than that of *Ca*GSTU1-1 (k_{cat}/K_m = 147.4 mM^{-1} min^{-1}), affirming a marked improvement in hydroperoxidase activity. Taken together, these results

Table 3
Steady-state kinetic analysis of *CaGm*GSTU for the CDNB/GSH and CuOOH/GSH and substrate systems and of *Ca*GSTU1-1 for the CuOOH/GSH system.

Enzyme	k_{cat} (min^{-1})	K_m (mM) (GSH)	K_m (mM) (CDNB)	k_{cat}/K_m (mM^{-1} min^{-1}) (GSH)	k_{cat}/K_m (mM^{-1} min^{-1}) (CDNB)
*CaGm*GSTU	1300 ± 28.5	0.60 ± 0.09	0.41 ± 0.04	2166.7	3170.7
Enzyme	**k_{cat} (min^{-1})**	**K_m (mM) (GSH)**	**K_m (mM) (CuOOH)**	**k_{cat}/K_m (mM^{-1} min^{-1}) (GSH)**	**k_{cat}/K_m (mM^{-1} min^{-1}) (CuOOH)**
*CaGm*GSTU	1470 ± 64.7	0.59 ± 0.11	3.40 ± 0.39	2491.5	432.4
*Ca*GSTU1-1	370 ± 12.3	0.30 ± 0.03	2.51 ± 0.23	1233.3	147.4

demonstrate that directed evolution successfully enhanced both the turnover rate and catalytic efficiency of the engineered *CaGm*GSTU without significantly compromising substrate affinity. The enzyme exhibited a 4-fold overall increase in hydroperoxidase activity compared to its parental form, consistent with its proposed role as a high-performance detoxification biocatalyst. These improvements are particularly significant given the environmental and physiological relevance of hydroperoxide detoxification.

Given the unchanged K_m values, the observed increase in k_{cat} likely reflects an alteration in the rate-limiting step of the enzymatic reaction. To explore this possibility, viscosity dependence assays were conducted to probe the role of diffusional constraints in the catalytic cycle. Previous studies suggest that the rate-limiting step in GSTs often involves product release or conformational transitions associated with diffusion (Ricci et al., 1996; Caccuri et al., 1996; Morgenstern, 2024). According to this model, if product release is diffusion-controlled, a linear relationship between the inverse relative rate constant (k^o_{cat}/k_{cat}), where k^o_{cat} is measured at standard viscosity η_0, and the relative viscosity (η/η_0) should be observed with a slope near unity. Conversely, if product release is governed by chemical or structural factors, the slope should approach zero.

As shown in Fig. 6, increasing the viscosity of the reaction medium led to a clear decrease in k_{cat} for the wild-type *Ca*GSTU1-1, yielding a slope of 0.61 ± 0.05 in the plot of relative viscosity (η/η^o) versus k^o_{cat}/k_{cat}. This result suggests that the rate-limiting step in the catalytic cycle is at least partially governed by diffusion-limited conformational rearrangements. In contrast, the *CaGm*GSTU variant exhibited a significantly lower slope of 0.31 ± 0.03 under identical conditions, indicating a reduced dependence on diffusional or structural transitions for

```
CaGSTU1-1     MADQVILLDFWPSPFGMRLRIALAEKGIEFEYREEDLRNKSPLLLQMNPIHKKIPVLVHN 60
CaGmGSTU      MADQVILLDFWPSPFGMRLRIALAEKGIKYEYKFEDLRNKSPLLLQMNPVHKKIPVLIHN 60
GmGSTU4-4     MSDEVVLLDFWPSPFGMRVRIALAEKGIKYEYKEEDLRNKSPLLLQMNPVHKKIPVLIHN 60

CaGSTU1-1     GKPICESLIAVQYIDEVWNHKSPLLPSDPYQRSQARFWADYVDKKIYDAGRNIWTKKGEE 120
CaGmGSTU      GKPICESLIAVQYIDEVWNHKSPLLPSDPYQRSQARFWADYVDKKIYDLGRKIWTSKGEE 120
GmGSTU4-4     GKPICESLIAVQYIEEVWNDRNPLLPSDPYQRAQTRFWADYVDKKIYDLGRKIWTSKGEE 120


CaGSTU1-1     QEAAKKEFIDALKLLEQELGDKTYFGGDKLGFVDVALIPFYTWFKGYETFGNFIVEKECP 180
CaGmGSTU      KEAAKKEFTEALKLLEQQLGDKTYFGGDKLGFVDVALIPFYTWFKGYETFGNFIVEKECP 180
GmGSTU4-4     KEAAKKEFIEALKLLEEQLGDKTYFGGDNLGFVDIALVPFYTWFKAYETFGTLNIESECP 180

CaGSTU1-1     KFIAWAKRCMQIESVSKSLPDQEKVYEFIVDIRKKIGIE 219
CaGmGSTU      KFIAWAKRCMQIESVSKSLPDQCKVYEFIMDLRKKIGIE 219
GmGSTU4-4     KFIAWAKRCLQKESVAKSLPDQQKVYEFIMDLRKKLGIE 219
```

Fig. 5. Sequence alignment of the chimeric *CaGm*GSTU variant with its parental isoenzymes *Ca*GSTU1-1 and *Gm*GSTU4-4. Amino acid sequences were aligned using CLUSTAL Omega (Sievers and Higgins, 2018). Regions of *CaGm*GSTU derived from *Gm*GSTU4-4 are highlighted in yellow, while segments originating from *Ca*GSTU1-1 are shown in green. Residues that are identical in both parent sequences are unshaded and conserved in *CaGm*GSTU. The alignment reflects the chimeric nature of *CaGm*GSTU as reconstructed from the nucleotide sequences of the respective genes used in DNA shuffling. (For interpretation of the references to color in this figure legend, the reader is referred to the Web version of this article.)

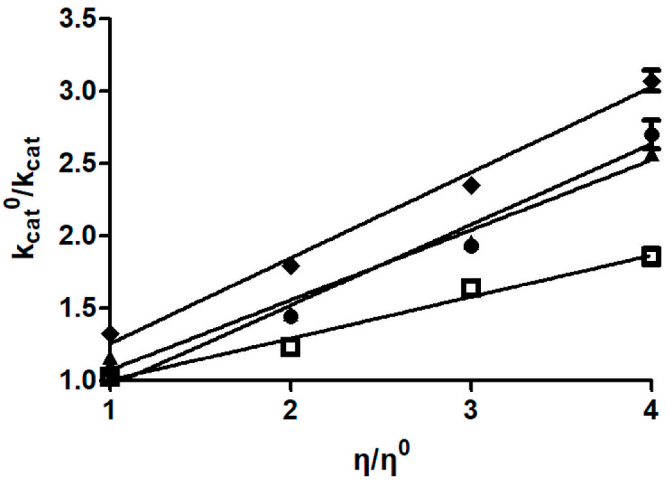

Fig. 6. Effect of solvent viscosity on catalytic turnover for the CDNB/GSH reaction catalyzed by *Ca*GSTUs and the *CaGm*GSTU variant. The reciprocal of the relative turnover number (k_{cat}^{o}/k_{cat}) is plotted against relative viscosity (η/η^{o}), adjusted by varying glycerol concentrations. Data are shown for *Ca*GSTU1-1 (●), *Ca*GSTU2-2 (▲), *Ca*GSTU3-3 (◆), and the engineered *CaGm*GSTU variant (□). Linear regression was applied to assess the viscosity dependence of each enzyme. All measurements were performed in triplicate, and values represent the mean of three independent experiments.

catalytic turnover. These findings imply that the engineered variant operates with a shifted or modified rate-limiting step, likely involving a more efficient product release mechanism that is less influenced by dynamic structural fluctuations.

This interpretation aligns with previous studies on *Gm*GSTU4-4 and related GSTs, which have identified α-helix 2 and the C-terminal α-helix 9 as key flexible elements modulating enzyme dynamics and influencing catalytic efficiency (Ricci et al., 1996; Caccuri et al., 1996). Structural alterations in these regions may underlie the observed shift in rate-limiting behavior in *CaGm*GSTU.

To further investigate the role of chemical reactivity in limiting the reaction rate, the impact of substrate structure was evaluated. Enzyme assays using CDNB and its brominated analogue (BDNB revealed that the wild-type *Ca*GSTU1-1 exhibited a specific activity ratio $(U/mg)^{CDNB}/(U/mg)^{BDNB} = 0.7$. In contrast, the corresponding ratio for *CaGm*GSTU was 1.15, suggesting a reversal in substrate preference. This shift is consistent with the lower electrophilicity of the bromo substituent and supports the conclusion that chemical reactivity plays a diminished role in the rate limiting step of the engineered variant. Collectively, these findings reinforce the idea that structural modifications in *CaGm*GSTU have altered the overall mechanism by relieving constraints on product release, thereby enhancing overall catalytic performance.

2.5. Structure prediction and analysis

Homology modeling was used to predict the three-dimensional structures of *Ca*GSTU1-1 and its engineered variant *CaGm*GSTU, providing a structural framework to contextualize the observed kinetic behaviors. The dimeric model of *Ca*GSTU1-1 bound to GSH is shown in Fig. 7A. Based on structural homology to *Gm*GSTU4-4 (Axarli et al., 2009b), critical amino acid residues constituting the hydrophobic substrate-binding site (H-site) were identified, including Phe10, Tyr107, Arg111, Trp114, and Ile212 (Fig. 7B). Similarly, residues critical for GSH binding (G-site) were mapped and include Ser13, Phe15, Arg18, Lys40, Lys53, Ile54, Ser67, and Lys104 (Fig. 7C). These residues are consistent with those previously implicated in substrate recognition and catalytic activity in Tau class GSTs (Axarli et al., 2009a, 2016).

Mapping the amino acid substitutions introduced through DNA shuffling revealed that most of the altered residues in *CaGm*GSTU are located outside the G- and H-sites, often at solvent-exposed positions (Fig. 7D). These peripheral locations suggest that most mutations are structurally neutral, exerting minimal direct influence on catalysis or substrate binding. However, one mutation, Ile212Leu, stands out as potentially functionally relevant. Residue 212 is situated within the C-terminal α-helix near the H-site, a region known to influence catalytic dynamics and substrate access (Axarli et al., 2016).

Analysis of non-covalent interactions indicates that Ile212 in *Ca*GSTU1-1 participates in 57 distinct interactions, whereas Leu212 in *CaGm*GSTU forms only 53. This reduction in contact number suggests a modest destabilization of the C-terminal helix, potentially increasing local flexibility. Given its proximity to the H-site, the Ile212Leu substitution may enhance dynamic motions in this region, contributing to the improved catalytic turnover observed in *CaGm*GSTU. This structural adaptation is consistent with the altered kinetic and viscosity-dependence profiles of the engineered variant.

To further explore the structural basis underlying the enhanced catalytic behavior of *CaGm*GSTU, the flexibility of key secondary structural elements was assessed through Normal Mode Analysis (NMA) using the DynaMut server (Rodrigues et al., 2018; https://biosig.lab.uq.edu.au/dynamut/). Particular focus was placed on the C-terminal α-helix 11, previously implicated in modulating enzyme dynamics (Fig. 1A). As shown in Fig. 7E, α-helix 11 exhibited the highest deformation energy among all structural elements, indicating a region of pronounced local flexibility. This was further supported by atomic fluctuation analysis (Fig. 7F), which revealed elevated amplitude of motion in this region, highlighting its dynamic nature. In addition to α-helix 11, the loop connecting α-helices 4 and 5 also demonstrated high flexibility and functional relevance. This loop influences the stability and movement of α-helix 4, which in turn contributes critical residues to the H-site, such as conserved tyrosine and arginine residues essential for substrate interaction (Fig. 7B). The vector field representation of the first non-trivial vibrational mode (Fig. 7G) illustrates large-scale coordinated movements centered around α-helix 11 and the α4–α5 loop, reinforcing their central role in the dynamic behavior of the enzyme. Furthermore, residue cross-correlation analysis (Fig. 7H) showed strong positive correlation in the motion of these regions, indicating that their fluctuations are synchronized in both phase and frequency.

Taken together, these findings suggest that the kinetic enhancements observed in *CaGm*GSTU are closely associated with altered flexibility in specific structural domains, particularly α-helix 11 and the α4–α5 loop. These dynamic regions appear to facilitate more efficient catalytic turnover and substrate processing by modulating access and movement at the active site.

2.6. Ligandin function

In addition to their well-established catalytic role, GSTs also perform a non-enzymatic function known as ligandin activity and bind a wide variety of endogenous and exogenous small hydrophobic molecules without catalyzing chemical transformation (Ma et al., 2024; Yuan et al., 2025). This binding typically occurs at the so-called L-site, a distinct non-catalytic site that often partially overlaps with or is adjacent to the G or H site of the enzyme (Schwartz et al., 2018).

To investigate the ligandin function, the binding and inhibitory effects of a range of pesticides on *Ca*GSTU1-1 and *CaGm*GSTU were examined, and the results are presented in Figs. 8 and 9 and listed in Table 4. The IC_{50} values for *CaGm*GSTU provide a direct assessment of the binding affinity between the pesticides and the enzyme. Across all tested pesticides, *CaGm*GSTU consistently exhibited lower IC_{50} values (Table 4), indicating increased sensitivity to inhibition and suggesting enhanced ligand-binding interactions. This is particularly evident in the case of tolclofos-methyl (Arena et al., 2018), where the IC_{50} of *CaGm*GSTU (78.4 ± 6.4 μM) was significantly lower than that of *Ca*GSTU1-1 (134.6 ± 14.7 μM), corresponding to a ~1.7-fold increase in inhibitory potency. Similarly, for pyraclostrobin, the IC_{50} was reduced

from 96.9 ± 2.2 μM in *Ca*GSTU1-1 to 53.7 ± 1.8 μM in *CaGm*GSTU, indicating a 1.8-fold enhancement in inhibitor binding. Another difference was observed with permethrin, where the IC_{50} dropped from 146.9 ± 7.5 μM to 93.6 ± 8.8 μM in the mutant, a reduction of over 35 %, further emphasizing the altered ligandin functionality of the engineered enzyme. The IC_{50} values for endosulfan and diflubenzuron were also lower in *CaGm*GSTU, though the differences were more modest.

Taken together, these data confirm that the directed evolution strategy not only enhanced catalytic activity but also altered the enzyme's xenobiotic-binding properties, particularly toward structurally diverse pesticides. These findings support the potential utility of *CaGm*GSTU in biosensing or bioremediation applications, where

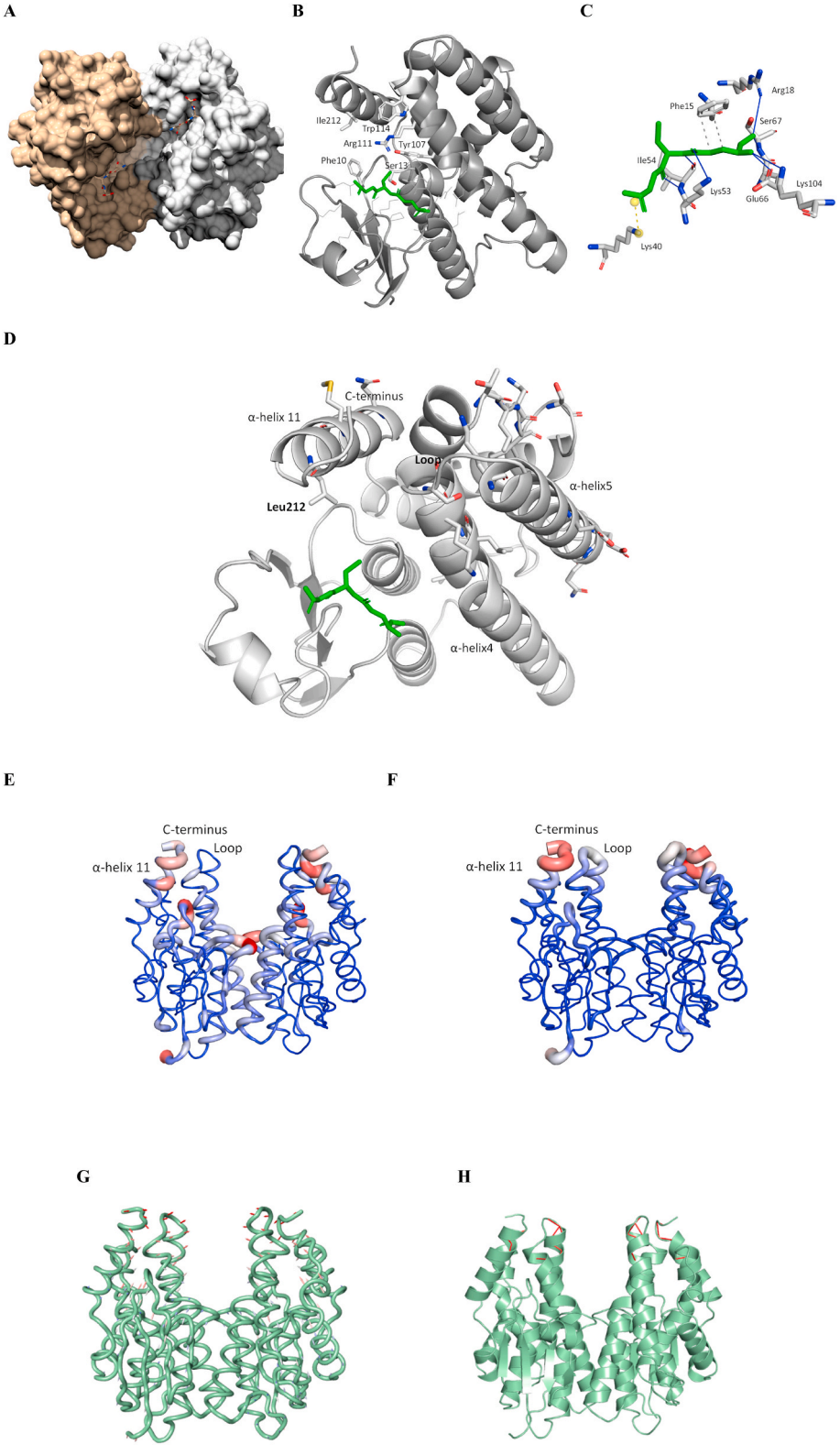

(caption on next page)

Fig. 7. Structural and dynamic analysis of *Ca*GSTU1-1 and the engineered *CaGm*GSTU variant. (A) Predicted surface model of *Ca*GSTU1-1 showing the dimeric structure with bound GSH represented as sticks and colored by atom type. **(B)** Key amino acid residues forming the hydrophobic substrate-binding site (H-site) are shown in stick representation and colored by atom type; GSH is highlighted in green. **(C)** Key residues comprising the GSH-binding site (G-site) are shown, with GSH in green. Hydrogen bonds are indicated by blue lines, hydrophobic interactions by dashed lines, and electrostatic interactions by yellow lines. **(D)** Predicted subunit structure of *CaGm*GSTU. Residues differing from the *Ca*GSTU1-1 parent sequence are depicted as sticks and colored by atom type. GSH is shown in green stick representation. **(E)** Deformation dynamics analysis of *CaGm*GSTU using DynaMut (Rodrigues et al., 2018). The magnitude of structural deformation is represented by tube thickness and color: blue (low), white (moderate), red (high). **(F)** Atomic fluctuation analysis of *CaGm*GSTU using DynaMut. Tube thickness and color represent the amplitude of atomic motion: blue (low), white (moderate), red (high). **(G)** Vector field representation of the first non-trivial normal mode of *CaGm*GSTU, highlighting large-scale dynamic motions, particularly in the C-terminal α-helix 11 and the α4–α5 loop. **(H)** Residue cross-correlation fluctuation map of *CaGm*GSTU. Highly correlated residue pairs (correlation coefficient $\geq$0.8) are shown in red, indicating synchronized dynamic behavior (Cab = 1: same period and phase; Cab = −1: same period, opposite phase; Cab = 0: no correlation). (For interpretation of the references to color in this figure legend, the reader is referred to the Web version of this article.)

increased sensitivity to environmental contaminants is advantageous.

Among the pesticides tested, tolclofos-methyl, a fungicide that inhibits phospholipid biosynthesis and is used to manage soil-borne diseases (Arena et al., 2018), showed the highest inhibition potency. Therefore, detailed inhibition kinetics analysis was performed to examine the interaction of tolclofos-methyl with *CaGm*GSTU. Fig. 10 depicts the Lineweaver-Burk double-reciprocal plots for the inhibition of *CaGm*GSTU by tolclofos-methyl. The results showed tolclofos-methyl behaved as a competitive inhibitor of GSH (Fig. 10A) and linear mixed-type inhibitor towards CDNB (Fig. 10C).

The inhibition constants determined from the secondary plots derived from Lineweaver–Burk data (Fig. 10B–D) and found 30.7 ± 2.5 μM and 46.5 ± 3.5 μM towards GSH and CDNB, respectively. The inhibition patterns observed suggest that tolclofos-methyl competes with GSH for binding at the enzyme's G-site. In contrast, the mixed-type inhibition observed with CDNB indicates that tolclofos-methyl can bind either to the free enzyme or to the enzyme-CDNB complex. This is consistent with the competitive inhibition mechanism observed for GSH. These data suggest that, at least in the case of tolclofos-methyl, the L-site of *CaGm*GSTU is located within or overlaps with the G-site.

3. Conclusions

This study reports the successful engineering of a novel GST variant, *CaGm*GSTU, through DNA shuffling of isoenzymes from *C. arietinum* and *G. max*. The engineered enzyme exhibited significantly enhanced catalytic efficiency, up to fourfold, towards model electrophilic substrates, along with improved hydroperoxidase activity and altered ligandin properties. Structural and kinetic analyses revealed that these functional gains were primarily driven by modifications in enzyme flexibility, particularly within dynamic regions critical for catalysis and substrate binding. Given the rising environmental and agricultural concerns associated with oxidative stress and pesticide contamination, *CaGm*GSTU represents a promising candidate for biotechnological applications in detoxification, stress tolerance enhancement, and sustainable crop protection strategies.

4. Experimental

4.1. Molecular cloning

Total RNA was extracted from *C. arietinum* tissues following the protocol established by Brusslan and Tobin (1992). First-strand cDNA synthesis was carried out using a commercial reverse transcription kit (Thermo Fisher Scientific), and the resulting cDNA was used as a template for the amplification of three GST isoenzymes, *Ca*GSTU1-1, *Ca*GSTU2-2, and *Ca*GSTU3-3. Gene-specific primers (listed in Table S1) were employed in PCR reactions conducted in a final volume of 50 μL, comprising 8 pmol of each primer, 0.5 μg of cDNA, 50 μM dNTPs, 5 μL of 10 × reaction buffer, and 1 unit of Taq DNA polymerase. The PCR conditions included an initial denaturation step, 30 amplification cycles (94 °C for 30 s, 55 °C for 30 s, 72 °C for 1 min), and a final elongation at 72 °C for 10 min. The amplified products were initially cloned into the pCR™ II-TOPO™ vector and subsequently re-amplified using the same primers to ensure the amplification of full-length open reading frames (ORFs). These amplicons were then directionally cloned into the pEXP5-CT/TOPO®TA vector for expression under control of the T7 promoter. All recombinant constructs were confirmed by DNA sequencing. The plasmid was transformed into chemically competent *E. coli* BL21 (DE3) cells for recombinant protein production.

4.2. Bioinformatics and structural analysis

Putative homologs of GSTs in *C. arietinum* were identified using the Phytozome database (https://phytozome-next.jgi.doe.gov/; *C. arietinum* v1.0, genome ID: 492), employing the amino acid sequence of the *Glycine max* GST isoenzyme *Gm*GSTU4-4 (UniProt ID: O49235) as a query. Multiple candidate sequences were retrieved and further evaluated through BLASTn searches against the NCBI expressed sequence tag (EST) databases. From these, three sequences showing expression under various abiotic stress conditions were selected for experimental characterization.

Multiple sequence alignment of the candidate *Ca*GSTU isoenzymes was performed using CLUSTAL Omega (Sievers and Higgins, 2018) and visualized with ESPript 3 (Robert and Gouet, 2014). Homology modelling of *Ca*GSTU1-1 and the engineered *CaGm*GSTU variant was carried out via the SWISS-MODEL server (Waterhouse et al., 2018), using the crystal structure of *Gm*GSTU4-4 (PDB ID: 4TOP; 82.65 % identity) as the structural template (Axarli et al., 2009b). Model reliability was assessed based on the Global Model Quality Estimate (GMQE), yielding values of 0.84 and 0.85 for *Ca*GSTU1-1 and *CaGm*GSTU, respectively. Structural accuracy was further supported by QMEAN scoring (Z-score: 0.81) (Benkert et al., 2011).

To examine molecular interactions, non-covalent contact analysis was performed using both the Protein Contacts Atlas (Kayikci et al., 2018) and the Arpeggio server (Jubb et al., 2017). Final model visualization, structural superposition, and interaction mapping were carried out using UCSF Chimera version 1.19 (Pettersen et al., 2004) and PyMOL (DeLano, 2002).

4.3. Expression and purification

Expression of *Ca*GSTU1-1, *Ca*GSTU2-2, and *Ca*GSTU3-3 enzymes was carried out in *E. coli* BL21 (DE3) cells, cultured at 37 °C in 1 L of LB medium containing 100 μg/mL ampicillin. *Ca*GSTU1-1 and *Ca*GSTU2-2 were purified by affinity chromatography using a GSH-Sepharose CL6B matrix activated with 1,4-butanediol diglycidyl ether. The column was pre-equilibrated with 20 mM potassium phosphate buffer (pH 7.0), and bound proteins were eluted with the same buffer containing 10 mM reduced GSH.

In contrast, *Ca*GSTU3-3 failed to bind to the affinity matrix, likely due to a low intrinsic affinity for immobilized GSH. As a result, purification was performed using ion-exchange chromatography on a DEAE-Sepharose CL6B column. The resin (1 mL) was equilibrated with 20 mM KH_2PO_4 buffer (pH 7.5), and the clarified cell lysate was applied to the column. After washing with 50 mL of the same buffer, bound

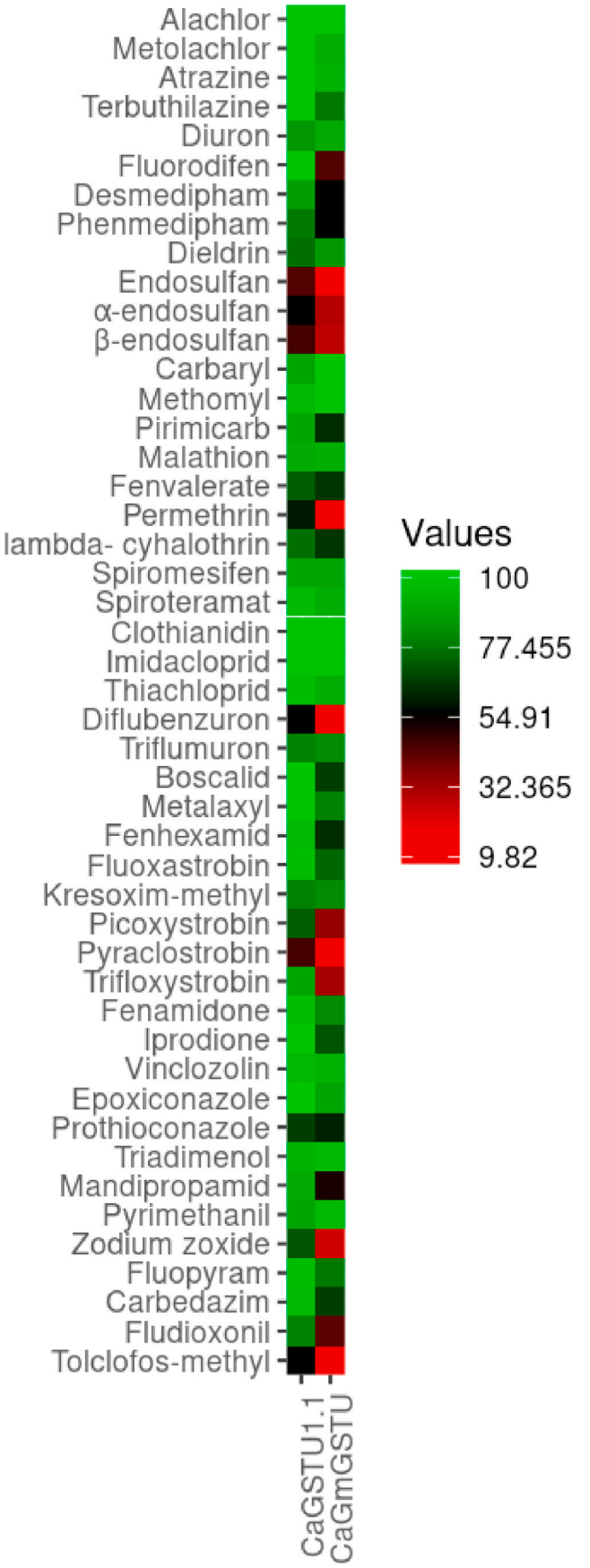

(caption on next column)

Fig. 8. Comparative screening of pesticide inhibition potency toward *Ca*GSTU1-1 and *CaGm*GSTU. The inhibitory effects of selected pesticides on *Ca*GSTU1-1 and *CaGm*GSTU were assessed using the standard CDNB–GSH assay. Inhibition percentages were calculated based on enzyme activity in the presence versus absence of each pesticide. Results are visualized as a heatmap, with color gradients indicating the mean inhibition values derived from three independent replicates. In all cases, standard deviations were below 8 %, indicating high reproducibility of the measurements. (For interpretation of the references to color in this figure legend, the reader is referred to the Web version of this article.)

proteins were eluted stepwise by increasing NaCl concentrations (50–500 mM). *Ca*GSTU3-3 eluted effectively at 150 mM NaCl.

4.4. Assay of enzyme activity, kinetics analysis and protein determination

Enzymatic activity was determined as previously described by Skopelitou et al. (2015). Electrophilic substrates were prepared in ethanol or acetonitrile, with final organic solvent concentrations in assay mixtures maintained between 2 % and 5 % (v/v). Reactions were conducted at a constant temperature using potassium phosphate buffer (0.1 M, pH 6.5), and initial reaction rates were measured in triplicate to ensure reproducibility. Initial velocity data were fitted to appropriate kinetic models, either the Michaelis-Menten or sigmoidal kinetics model (Axarli et al., 2016), using non-linear regression analysis in GraphPad Prism (version 5.0) to derive the kinetic parameters. Protein quantification was performed using the Bradford method with BSA as the reference standard (Kielkopf et al., 2020).

4.5. DNA shuffling and activity screening

Directed evolution was carried out using the isoenzymes *Ca*GSTU1-1 from *C. arietinum* and *Gm*GSTU4-4 from *Glycine* max as parental sequences, following the DNA shuffling protocol described by Axarli et al. (2016), with minor modifications. Equal quantities (1:1 ratio) of the expression plasmids encoding *Ca*GSTU1-1 and *Gm*GSTU4-4 were mixed to a final DNA concentration of approximately 2 μg. The mixture was subjected to limited DNase I digestion (0.5 U in 50 μL with 10 × DNase buffer) to generate fragments ranging from 50 to 100 bp. Digestion was performed at multiple time intervals (0, 4, 6, 8, 12, and 15 min) and terminated by heat inactivation at 65 °C for 10 min, followed by addition of stop buffer (0.1 mM EDTA final concentration). Fragmentation efficiency was assessed by electrophoresis on a 2 % (w/v) agarose gel.

Random reassembly of DNA fragments was conducted using primerless PCR with Kapa HiFi polymerase. Reaction products from the 8-, 12-, and 15-min digestions were used as templates. The thermal cycling protocol for reassembly included an initial denaturation at 96 °C for 3 min, followed by 40 cycles consisting of 94 °C for 30 s, 55 °C for 1 min, and 72 °C for 1 min, with a final elongation step at 72 °C for 7 min. The reassembled genes were subsequently amplified by PCR using gene-specific primers for *Ca*GSTU1-1 and *Gm*GSTU4-4, and a polymerase mix (Kapa HiFi and Kapa Taq, 1:1). Amplification was performed using the same cycling protocol as above. The resulting full-length chimeric genes were confirmed by 1 % (w/v) agarose gel electrophoresis, then cloned into the T7 expression vector pEXP5-CT/TOPO®TA. Following sequence verification, the constructs were transformed into *E. coli* BL21 (DE3) for expression. The resulting library was functionally screened for GST activity using the CDNB/GSH substrate system, as previously described (Axarli et al., 2016).

4.6. Thermal stability

The thermal stability of *Ca*GSTU isoenzymes and the engineered *CaGm*GSTU variant was assessed by incubating the purified enzymes at temperatures ranging from 4 °C to 80 °C for 10 min in 0.1 M potassium phosphate buffer (pH 7.0). Following heat treatment, residual enzymatic

Table 4
IC_{50} values for the wild-type *Ca*GSTU1-1 and the *CaGm*GSTU variant with pesticides with the highest inhibition potency.

Xenobiotic	Enzyme	IC_{50} (μM)
Endosulfan	*Ca*GSTU1-1	63.2 ± 5.8
	*CaGm*GSTU	56.7 ± 4.8
Permethrin	*Ca*GSTU1-1	146.9 ± 7.5
	*CaGm*GSTU	93.6 ± 8.8
Tolclofos-methyl	*Ca*GSTU1-1	1,34.6 ± 14.7
	*CaGm*GSTU	78.4 ± 6.4
Diflubenzuron	*Ca*GSTU1-1	83.7 ± 3.9
	*CaGm*GSTU	67.2 ± 2.7
Pyraclostrobin	*Ca*GSTU1-1	96.9 ± 2.2
	*CaGm*GSTU	53.7 ± 1.8

activity was determined using standard activity assays. To determine the melting temperature (Tm), defined as the temperature corresponding to a 50 % reduction in initial enzyme activity, relative residual activity (%) was plotted as a function of temperature (°C). Data were analyzed and T_m values derived using GraphPad Prism software (version 5.0).

4.7. Viscosity dependence of kinetic parameters

To investigate the influence of solvent viscosity on catalytic efficiency, kinetic assays for *Ca*GSTU isoenzymes and the *CaGm*GSTU variant were conducted at 37 °C in 0.1 M potassium phosphate buffer (pH 6.5) supplemented with increasing concentrations of glycerol (0–40 % v/v). Enzymatic activities were then measured under each condition to evaluate the correlation between viscosity and kinetic parameters.

CRediT authorship contribution statement

Anni Kontouri: Writing – original draft, Methodology, Investigation. **Nikolaos Georgakis:** Writing – review & editing, Methodology, Formal analysis. **Anastassios C. Papageorgiou:** Writing – original draft, Investigation. **Nikolaos E. Labrou:** Writing – review & editing, Writing – original draft, Supervision, Investigation, Conceptualization.

Declaration of competing interest

The authors declare that they have no known competing financial interests or personal relationships that could have appeared to influence

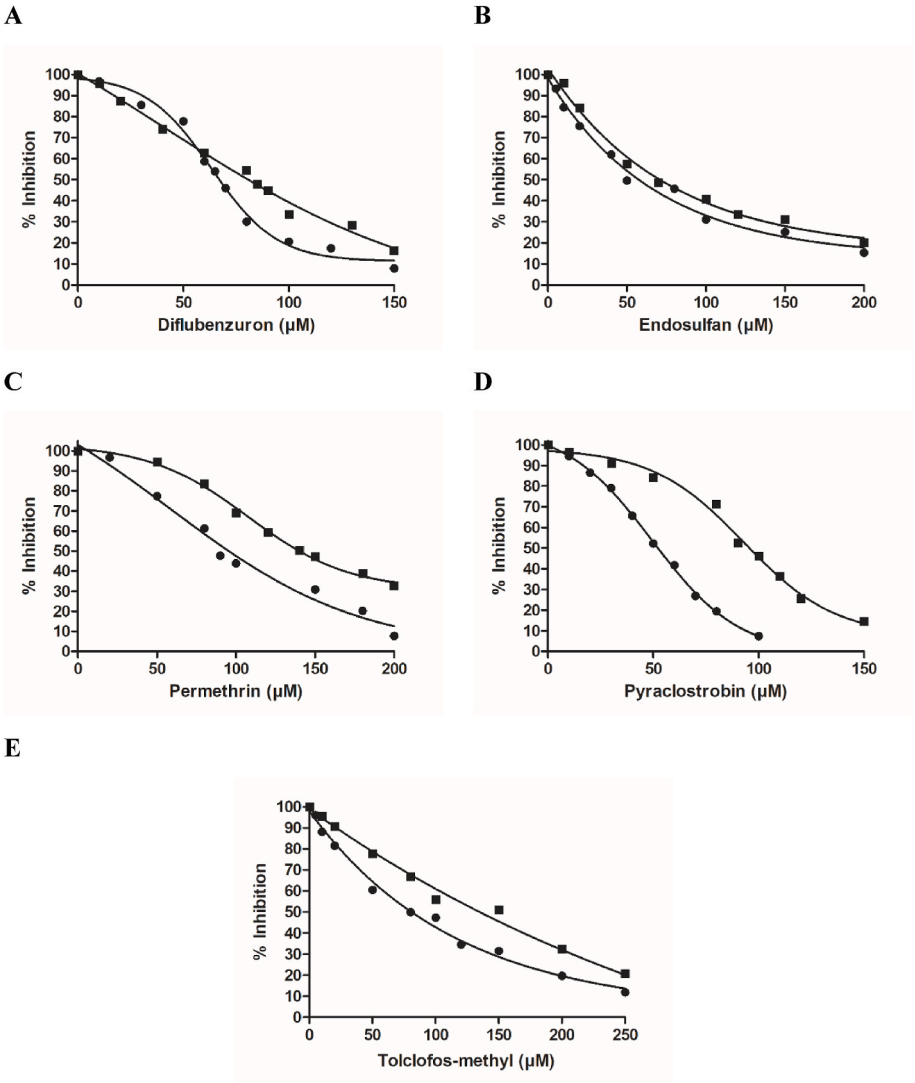

Fig. 9. Dose–response curves for the inhibition of *Ca*GSTU1-1 and *CaGm*GSTU by selected pesticides. The inhibitory effects of five representative pesticides on *Ca*GSTU1-1 (●) and *CaGm*GSTU (■) were evaluated by measuring residual enzymatic activity using the CDNB–GSH assay at increasing inhibitor concentrations. Dose–response curves are shown for: **(A)** diflubenzuron, **(B)** endosulfan, **(C)** permethrin, **(D)** pyraclostrobin, and **(E)** tolclofos-methyl. Each point represents the mean of three independent measurements.

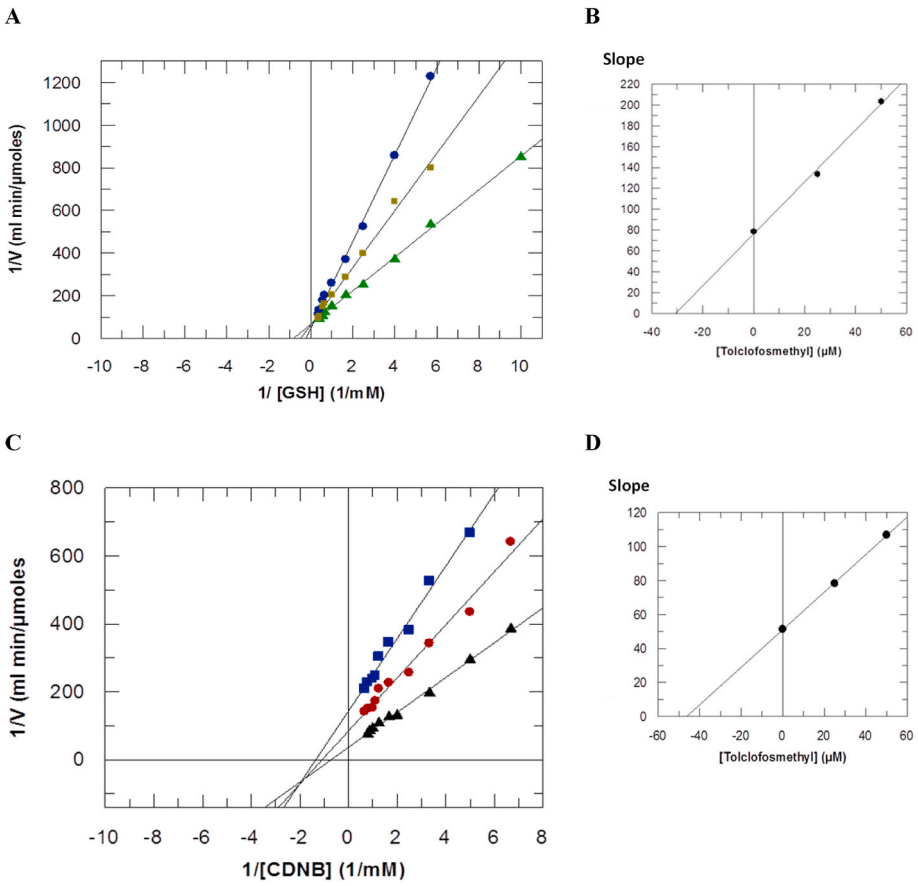

Fig. 10. Kinetic inhibition analysis of *CaGm*GSTU by tolclofos-methyl. (A) Lineweaver–Burk plot showing the effect of tolclofos-methyl on *CaGm*GSTU activity at varying concentrations of GSH. Tolclofos-methyl concentrations were 0 µM (▲), 25 µM (■), and 50 µM (●). **(B)** Secondary plot derived from panel A, illustrating the relationship between the slopes (K_m/V_{max}) of the Lineweaver–Burk plots and the inhibitor concentration. The inhibition constant (K_i) was determined from the x-axis intercept. **(C)** Lineweaver–Burk plot showing the effect of tolclofos-methyl on *CaGm*GSTU activity at varying concentrations of CDNB. Inhibitor concentrations were 0 µM (▲), 25 µM (●), and 50 µM (■). **(D)** Secondary plot corresponding to panel C, used to calculate the K_i value from the linear regression of slope versus inhibitor concentration. Each experiment was conducted in triplicate, and values represent mean activity from three independent replicates.

the work reported in this paper.

Acknowledgements

AK and NEL acknowledge financial support from the grant program THALES, co-funded by the European Union – European Social Fund and National Resources.

Appendix A. Supplementary data

Supplementary data to this article can be found online at https://doi.org/10.1016/j.phytochem.2025.114692.

Data availability

GenBank accession numbers for the sequences are as follows: *Ca*GSTU1-1 (ALZ41811.1), *Ca*GSTU2-2 (ALZ41812.1), and *Ca*GSTU3-3 (ALZ41813.1).

References

Akchaya, K., Parasuraman, P., Kannan, Pandian, Vijayakumar, S., Thirukumaran, K., Firnass, Mustaffa Mohamed Roshan Abu, Kumar, Rajpoot Sudhir, Choudhary, Anil K., 2025. Boosting resource use efficiency, soil fertility, food security, ecosystem services, and climate resilience with legume intercropping: a review. Front. Sustain. Food Syst. 9. https://doi.org/10.3389/fsufs.2025.1527256.

Arena, M., Auteri, D., Barmaz, S., Bellisai, G., Brancato, A., Brocca, D., Bura, L., Byers, H., Chiusolo, A., Court Marques, D., Crivellente, F., De Lentdecker, C., Egsmose, M., Erdos, Z., Fait, G., Ferreira, L., Goumenou, M., Greco, L., Ippolito, A., Istace, F., Jarrah, S., Kardassi, D., Leuschner, R., Lythgo, C., Magrans, J.O., Medina, P., Miron, I., Molnar, T., Nougadere, A., Padovani, L., Parra Morte, J.M., Pedersen, R., Reich, H., Sacchi, A., Santos, M., Serafimova, R., Sharp, R., Stanek, A., Streissl, F., Sturma, J., Szentes, C., Tarazona, J., Terron, A., Theobald, A., Vagenende, B., Verani, A., Villamar-Bouza, L., 2018. Peer review of the pesticide risk assessment of the active substance tolclofos-methyl. EFSA J. 16, e05130. https://doi.org/10.2903/j.efsa.2018.5130.

Arnold, F.H., 1998. Design by directed evolution. Acc. Chem. Res. 31, 125–131. https://doi.org/10.1021/ar960017f.

Asati, R., Tripathi, M.K., Yadav, R.K., Tripathi, N., Sikarwar, R.S., Tiwari, P.N., 2024. Investigation of drought stress on Chickpea (*Cicer arietinum* L.) genotypes employing various physiological enzymatic and non-enzymatic biochemical parameters. Plants 13, 2746. https://doi.org/10.3390/plants13192746.

Axarli, I., Ataya, F., Labrou, N.E., 2023. Repurposing glutathione transferases: directed evolution combined with chemical modification for the creation of a semisynthetic enzyme with high hydroperoxidase activity. Antioxidants 13, 41. https://doi.org/10.3390/antiox13010041.

Axarli, I., Dhavala, P., Papageorgiou, A.C., Labrou, N.E., 2009a. Crystal structure of Glycine max glutathione transferase in complex with glutathione: investigation of the mechanism operating by the Tau class glutathione transferases. Biochem. J. 422, 247–256. https://doi.org/10.1042/BJ20090224.

Axarli, I., Dhavala, P., Papageorgiou, A.C., Labrou, N.E., 2009b. Crystallographic and functional characterization of the fluorodifen-inducible glutathione transferase from Glycine max reveals an active site topography suited for diphenylether herbicides and a novel L-site. J. Mol. Biol. 385, 984–1002. https://doi.org/10.1016/j.jmb.2008.10.084.

Axarli, I., Muleta, A.W., Chronopoulou, E.G., Papageorgiou, A.C., Labrou, N.E., 2017. Directed evolution of glutathione transferases towards a selective glutathione-binding site and improved oxidative stability. Biochim. Biophys. Acta Gen. Subj. 1861, 3416–3428. https://doi.org/10.1016/j.bbagen.2016.09.004.

Axarli, I., Muleta, A.W., Vlachakis, D., Kossida, S., Kotzia, G., Maltezos, A., Dhavala, P., Papageorgiou, A.C., Labrou, N.E., 2016. Directed evolution of Tau class glutathione transferases reveals a site that regulates catalytic efficiency and masks co-operativity. Biochem. J. 473, 559–570. https://doi.org/10.1042/BJ20150930.

Benkert, P., Biasini, M., Schwede, T., 2011. Toward the estimation of the absolute quality of individual protein structure models. Bioinformatics 27, 343–350. https://doi.org/10.1093/bioinformatics/btq662.

Brusslan, J.A., Tobin, E.M., 1992. Light-independent developmental regulation of cab gene expression in Arabidopsis thaliana seedlings. Proc. Natl. Acad. Sci. USA. 89, 7791–7795. https://doi.org/10.1073/pnas.89.16.7791.

Caccuri, A.M., Ascenzi, P., Antonini, G., Parker, M.W., Oakley, A.J., Chiessi, E., Nuccetelli, M., Battistoni, A., Bellizia, A., Ricci, G., 1996. Structural flexibility modulates the activity of human glutathione transferase P1-1. Influence of a poor co-substrate on dynamics and kinetics of human glutathione transferase. J. Biol. Chem. 271, 16193–16198. https://doi.org/10.1074/jbc.271.27.16193.

Cassier-Chauvat, C., Marceau, F., Farci, S., Ouchane, S., Chauvat, F., 2023. The glutathione system: a journey from cyanobacteria to higher eukaryotes. Antioxidants 12, 1199. https://doi.org/10.3390/antiox12061199.

Chronopoulou, E.G., Papageorgiou, A.C., Ataya, F., Nianiou-Obeidat, I., Madesis, P., Labrou, N.E., 2018. Expanding the plant GSTome through directed evolution: DNA shuffling for the generation of new synthetic enzymes with engineered catalytic and binding properties. Front. Plant Sci. 9, 1737. https://doi.org/10.3389/fpls.2018.01737.

DeLano, L.W., 2002. PyMOL: an open-source molecular graphics tool. Ccp4 Newsletter on Protein Crystallography, 40, pp. 82–94.

Dixon, D.P., Lapthorn, A., Edwards, R., 2002. Plant glutathione transferases. Genome Biol. 3 (3), reviews3004.1. https://doi.org/10.1186/gb-2002-3-3-reviews3004.

Dixon, D.P., McEwen, A.G., Lapthorn, A.J., Edwards, R., 2003. Forced evolution of a herbicide detoxifying glutathione transferase. J. Biol. Chem. 278, 23930–23935. https://doi.org/10.1074/jbc.M303620200.

Gallé, Á., Bela, K., Hajnal, Á., Faragó, N., Horváth, E., Horváth, M., Puskás, L., Csiszár, J., 2021. Crosstalk between the redox signalling and the detoxification: GSTs under redox control? Plant Physiol. Biochem. 169, 149–159. https://doi.org/10.1016/j.plaphy.2021.11.009.

Han, X.M., Yang, Z.L., Liu, Y.J., Yang, H.L., Zeng, Q.Y., 2018. Genome-wide profiling of expression and biochemical functions of the Medicago glutathione S-transferase gene family. Plant Physiol. Biochem. 126, 126–133. https://doi.org/10.1016/j.plaphy.2018.03.004.

Hasan, M.S., Singh, V., Islam, S., Islam, M.S., Ahsan, R., Kaundal, A., Islam, T., Ghosh, A., 2021. Genome-wide identification and expression profiling of glutathione S-transferase family under multiple abiotic and biotic stresses in *Medicago truncatula* L. PLoS One 16 (2), e0247170. https://doi.org/10.1371/journal.pone.0247170.

Horváth, E., Kulman, K., Tompa, B., Hajnal, Á.B., Pelsőczi, A., Bela, K., Gallé, Á., Csiszár, J., 2023. Glutathione transferases are involved in the genotype-specific salt-stress response of tomato plants. Antioxidants 12, 1682. https://doi.org/10.3390/antiox12091682.

Ioannou, E., Papageorgiou, A.C., Labrou, N.E., 2022. Directed evolution of phi class glutathione transferases involved in multiple-herbicide resistance of grass weeds and crops. Int. J. Mol. Sci. 23, 7469. https://doi.org/10.3390/ijms23137469.

Jubb, H.C., Higueruelo, A.P., Ochoa-Montaño, B., Pitt, W.R., Ascher, D.B., Blundell, T.L., 2017. Arpeggio: a web server for calculating and visualising interatomic interactions in protein structures. J. Mol. Biol. 429, 365–371. https://doi.org/10.1016/j.jmb.2016.12.004.

Kaur, G., Sanwal, S.K., Sehrawat, N., Kumar, A., Kumar, N., Mann, A., 2022. Getting to the roots of Cicer arietinum L. (Chickpea) to study the effect of salinity on morpho-physiological, biochemical and molecular traits. Saudi J. Biol. Sci. 29, 103464. https://doi.org/10.1016/j.sjbs.2022.103464.

Kayikci, M., Venkatakrishnan, A.J., Scott-Brown, J., Ravarani, C.N.J., Flock, T., Babu, M. M., 2018. Visualization and analysis of non-covalent contacts using the protein contacts atlas. Nat. Struct. Mol. Biol. 25, 185–194. https://doi.org/10.1038/s41594-017-0019-z.

Kielkopf, C.L., Bauer, W., Urbatsch, I.L., 2020. Bradford assay for determining protein concentration. Cold Spring Harb. Protoc. 2020, 102269. https://doi.org/10.1101/pdb.prot102269.

Kontouri, A., Ataya, F.S., Madesis, P., Labrou, N.E., 2024. Comparative characterization of three homologous glutathione transferases from the weed Lolium perenne. Foods 13, 3584. https://doi.org/10.3390/foods13223584.

Kumar, S., Stecher, G., Suleski, M., Sanderford, M., Sharma, S., Tamura, K., 2024. MEGA12: molecular evolutionary genetic analysis version 12 for adaptive and green computing. Mol. Biol. Evol. 41 (12), msae263. https://doi.org/10.1093/molbev/msae263.

Labrou, N.E., Papageorgiou, A.C., Pavli, O., Flemetakis, E., 2015. Plant GSTome: structure and functional role in xenome network and plant stress response. Curr. Opin. Biotechnol. 32, 186–194. https://doi.org/10.1016/j.copbio.2014.12.024.

Lallement, P.A., Brouwer, B., Keech, O., Hecker, A., Rouhier, N., 2014. The still mysterious roles of cysteine-containing glutathione transferases in plants. Front. Pharmacol. 5, 192. https://doi.org/10.3389/fphar.2014.00192.

Letunic, I., Bork, P., 2021. Interactive tree of life (iTOL) v5: an online tool for phylogenetic tree display and annotation. Nucleic Acids Res. 49 (W1), W293–W296. https://doi.org/10.1093/nar/gkab301.

Liu, T., Du, Q., Li, S., Yang, J., Li, X., Xu, J., Chen, P., Li, J., Hu, X., 2019. GSTU43 gene involved in ALA-regulated redox homeostasis, to maintain coordinated chlorophyll synthesis of tomato at low temperature. BMC Plant Biol. 19, 323. https://doi.org/10.1186/s12870-019-1929-1.

Ma, S., Qi, Y., Ma, J., Wang, Y., Feng, G., Huang, L., Nie, G., Zhang, X., 2024. Functional characterization of TrGSTF15, a glutathione S-transferase gene family member, on the transport and accumulation of anthocyanins and proanthocyanidins in Trifolium repens. Plant Physiol. Biochem. 215, 109038. https://doi.org/10.1016/j.plaphy.2024.109038.

Mannervik, B., 2023. Versatility of glutathione transferase proteins. Biomolecules 13, 1749. https://doi.org/10.3390/biom13121749.

Micic, N., Holmelund Rønager, A., Sørensen, M., Bjarnholt, N., 2024. Overlooked and misunderstood: can glutathione conjugates be clues to understanding plant glutathione transferases? Philos. Trans. R. Soc. Lond. B Biol. Sci. 379, 20230365. https://doi.org/10.1098/rstb.2023.0365.

Morgenstern, R., 2024. Kinetic behavior of glutathione transferases: understanding cellular protection from reactive intermediates. Biomolecules 14, 641. https://doi.org/10.3390/biom14060641.

Neuefeind, T., Reineme, r P., Bieseler, B., 1997. Plant glutathione S-transferases and herbicide detoxification. Biol. Chem. 378, 199–205. PMID: 9165071.

Oakley, A., 2011. Glutathione transferases: a structural perspective. Drug Metab. Rev. 43, 138–151. https://doi.org/10.3109/03602532.2011.558093.

Perperopoulou, F., Pouliou, F., Labrou, N.E., 2018. Recent advances in protein engineering and biotechnological applications of glutathione transferases. Crit. Rev. Biotechnol. 38, 511–528. https://doi.org/10.1080/07388551.2017.1375890.

Pettersen, E.F., Goddard, T.D., Huang, C.C., Couch, G.S., Greenblatt, D.M., Meng, E.C., Ferrin, T.E., 2004. UCSF Chimera–a visualization system for exploratory research and analysis. J. Comput. Chem. 25, 1605–1612. https://doi.org/10.1002/jcc.20084.

Reetz, M.T., Wang, L.W., Bocola, M., 2006. Directed evolution of enantioselective enzymes: iterative cycles of CASTing for probing protein-sequence space. Angew. Chem. Int. Ed. 45, 1236–1241. https://doi.org/10.1002/anie.200502746.

Ricci, G., Caccuri, A.M., Lo Bello, M., Rosato, N., Mei, G., Nicotra, M., Chiessi, E., Mazzetti, A.P., Federici, G., 1996. Structural flexibility modulates the activity of human glutathione transferase P1-1. Role of helix 2 flexibility in the catalytic mechanism. J. Biol. Chem. 271, 16187–16192. https://doi.org/10.1074/jbc.271.27.16187.

Robert, X., Gouet, P., 2014. Deciphering key features in protein structures with the new ENDscript server. Nucleic Acids Res. 42, W320–W324. https://doi.org/10.1093/nar/gku316.

Rodrigues, C.H., Pires, D.E., Ascher, D.B., 2018. DynaMut: predicting the impact of mutations on protein conformation, flexibility and stability. Nucleic Acids Res. 46, W350–W355. https://doi.org/10.1093/nar/gky300.

Roxas, V.P., Lodhi, S.A., Garrett, D.K., Mahan, J.R., Allen, R.D., 2000. Stress tolerance in transgenic tobacco seedlings that overexpress glutathione S-transferase/glutathione peroxidase. Plant Cell Physiol. 41, 1229–1234. https://doi.org/10.1093/pcp/pcd051.

Schwartz, M., Perrot, T., Aubert, E., Dumarçay, S., Favier, F., Gérardin, P., Morel-Rouhier, M., Mulliert, G., Saiag, F., Didierjean, C., Gelhaye, E., 2018. Molecular recognition of wood polyphenols by phase II detoxification enzymes of the white rot Trametes versicolor. Sci. Rep. 8, 8472. https://doi.org/10.1038/s41598-018-26601-3.

Sievers, F., Higgins, D.G., 2018. Clustal Omega for making accurate alignments of many protein sequences. Protein Sci. 27, 135–145. https://doi.org/10.1002/pro.3290.

Silva, B.Q., da Silva, M.N., Smetana, S., Vasconcelos, M.W., 2025. Comparative environmental and nutritional sustainability analysis of Kabuli and Desi Chickpea (*Cicer arietinum* L.) types at the farm and product level. J. Clean. Prod. 513, 145706. https://doi.org/10.1016/j.jclepro.2025.145706.

Skopelitou, K., Muleta, A.W., Papageorgiou, A.C., Chronopoulou, E., Labrou, N.E., 2015. Catalytic features and crystal structure of a tau class glutathione transferase from *Glycine max* specifically upregulated in response to soybean mosaic virus infections. Biochim. Biophys. Acta 1854, 166–177. https://doi.org/10.1016/j.bbapap.2014.11.008.

Sylvestre-Gonon, E., Law, S.R., Schwartz, M., Robe, K., Keech, O., Didierjean, C., Dubos, C., Rouhier, N., Hecker, A., 2019. Functional, structural and biochemical features of plant Serinyl-Glutathione transferases. Front. Plant Sci. 10, 608. https://doi.org/10.3389/fpls.2019.00608.

Verma, M., Kumar, V., Patel, R.K., Garg, R., Jain, M., 2015. CTDB: an integrated chickpea transcriptome database for functional and applied genomics. PLoS One 10, e0136880. https://doi.org/10.1371/journal.pone.0136880.

Waterhouse, A., Bertoni, M., Bienert, S., Studer, G., Tauriello, G., Gumienny, R., Heer, F. T., de Beer, T.A.P., Rempfer, C., Bordoli, L., Lepore, R., Schwede, T., 2018. SWISS-MODEL: homology modelling of protein structures and complexes. Nucleic Acids Res. 46, W296–W303. https://doi.org/10.1093/nar/gky427.

Xu, J., Jiang, H., Cao, Q., Li, Y., Kuang, X., Wu, Y., Chai, Y., Li, J., Lu, K., Wei, L., 2025. The glutathione S-transferase BnGSTU12 enhances the resistance of Brassica napus to Sclerotinia sclerotiorum through reactive oxygen species homeostasis and jasmonic acid signaling. Plant Physiol. Biochem. 219, 109446. https://doi.org/10.1016/j.plaphy.2024.109446.

Yuan, M., Wei, X., Peng, F., Wang, Q., Zhoum, L., Wang, Y., 2025. PdGSTF1, PdGSTU3, and PdGSTU5 are essential for the accumulation of isosalipurposide and other pigments in peonies. Plant J. 122, e70178. https://doi.org/10.1111/tpj.70178.

Zhang, Y., Farhan, M., Yangm, H., Zhao, J., Ma, X., Zhang, S., 2025. Genome-wide analyses of glutathione S-transferase gene family and expression profiling among three haplotypes Aphis gossypii. Comp. Biochem. Physiol., Part D: Genomics Proteomics 54, 101416. https://doi.org/10.1016/j.cbd.2025.101416.

Zimmermann, P., Hirsch-Hoffmann, M., Hennig, L., Gruissem, W., 2004. Genevestigator. Arabidopsis microarray database and analysis toolbox. Plant Physiol. 136, 2621–2632. https://doi.org/10.1104/pp.104.046367.